Heliyon 10 (2024) e30541

Contents lists available at ScienceDirect

Heliyon

journal homepage: www.cell.com/heliyon

Research article

Exploration of rice husk ash as a green corrosion inhibitor immersed in NH_4Cl 7.5 % solution

Agus Paul Setiawan Kaban [a], Johny Wahyuadi Soedarsono [a,*], Mochammad Syaiful Anwar [b], Wahyu Mayangsari [b], Ahmad Maksum [c], Aga Ridhova [b], Rini Riastuti [a], Dedy Iskandar [d], Ayende [e]

[a] *Prof Johny Wahyuadi Laboratory, Department of Metallurgical and Materials Engineering, Universitas Indonesia, Depok, 16424, Indonesia*
[b] *Research Center for Metallurgy-National Research and Innovation Agency, Kawasan Sains Dan Teknologi BJ Habibie, Tangerang Selatan, Banten, 15314, Indonesia*
[c] *Department of Mechanical Engineering, Politeknik Negeri Jakarta, Jl. Professor Doktor G.A. Siwabessy, Kukusan, Kecamatan Beji, Depok, 16425, Indonesia*
[d] *Pertamina Hulu Indonesia, Graha Elnusa Lantai 7, Jl. TB Simatupang, RT.10/RW.3, Cilandak Tim., Ps. Minggu, Kota Jakarta Selatan, Daerah Khusus Ibukota, Jakarta, 12560, Indonesia*
[e] *Department of Mechanical Refinery Engineering PEM Akamigas, Jl. Gajah Mada No. 38, Cepu Blora Jawa Tengah, Indonesia*

ARTICLE INFO

Keywords:
Green corrosion inhibitor
Rice husk ash
Liquid smoke inhibitor
Atmospheric corrosion
NH_4Cl corrosion protection

ABSTRACT

The study reports the development of a liquid smoke solution of rice husk ash (RHA) as a green corrosion inhibitor in NH_4Cl solution in approaching corrosion protection for refinery facilities. The recent utilization of RHA has a partial solution to address the possible chemical to form a filming layer to disconnect bare metal and their environment. This work prepared the RHA solution by condensing the RHA vapor before adding it to various concentrations. The corrosion test of potentiodynamic and electrochemicals intends to discover the inhibitor's corrosion resistance before examining the electronic transition corresponding to the contribution of several functional groups using Ultraviolet Visible (UV–Vis) and Fourier-Transform Infrared Spectroscopy (FTIR). Surface evaluation intends to unveil the nature of the corrosion by utilizing the Scanning Electronic and Atomic Force Microscope. The corrosion test result shows the depression of corrosion rate to 0.120 mmpy with high efficiency beyond 96 % in the addition of 7.5 ppm RHA inhibitor. The greater Nyquist semicircle diameter at high concentrations increases the adsorption of the RHA on the surface of C1018. The electronic transition of n–π* and π –π* shows an extensive contribution of C═C, C═O, and –OH based on the UV–Vis and FTIR test. The formation of a complex compound of Fe-$(NH_4Cl\text{-}RHA)_n$ blocks the corrosion active sites to reduce the corrosion. This study paves the way for using RHA as an organic compound under NH_4Cl conditions, such as in a refinery process facility.

* Corresponding author.
E-mail addresses: agus.paul@ui.ac.id (A.P.S. Kaban), jwsono@metal.ui.ac.id (J.W. Soedarsono), moch031@brin.go.id (M.S. Anwar), wahy049@brin.go.id (W. Mayangsari), ahmad.maksum@mesin.pnj.ac.id (A. Maksum), agaridhova@gmail.com (A. Ridhova), riastuti@metal.ui.ac.id (R. Riastuti), dedy.iskandar1@pertamina.com (D. Iskandar), ayende@esdm.go.id (Ayende).

https://doi.org/10.1016/j.heliyon.2024.e30541
Received 12 October 2023; Received in revised form 16 April 2024; Accepted 29 April 2024
Available online 6 May 2024

1. Introduction

The petroleum refinery industry is a complex system that provides various hydrocarbon energy-based products, including plastics, polymers, and kerosene, mainly produced from the extensive process in the refining industry [1]. The refinery conversion process changes the crude oil fraction at the level of molecules geared toward valuable commodities. Because of their complexity and high pressure and temperature variation, the equipment is prone to various types of corrosion, including the plague of NH_4Cl [2]. In the heat exchanger tube, the formation of solid NH_4Cl at higher temperatures causes water vapor. In comparison, at lower temperatures, the deposition of NH_4Cl allows extensive salt deposition in the inner surface of equipment and pipping. It is reported that the risk of corrosion has reached nearly two times the folds compared to the corrosion mitigation fund in 2013 [3], while it imposes another US$ 3 trillion to impede corrosion. Hence, the equipment protection against the material's degradation is expensive and critical to depress the business and environmental loss including injecting corrosion inhibitors.

Corrosion inhibitors work through the adsorption of their active molecules at the interface to separate the corrodents and the metal and inhibit the electrochemical process on the metallic surface [4]. However, the recent types of inhibitors pose drawbacks, including their biodegradability, toxin accumulation, cost, and chemical availability, which have recently imposed higher expenses for production. The inhibitor's polarity is another key to unveiling the possible use of natural inhibitors to address the stability adsorption process of inhibitors. Therefore, urgent efforts are required to seek and select suitable inhibitors for the refinery.

Green corrosion inhibitors (GCI) are in demand to provide a solution for the impetus search for organic inhibitors, exclusively to remedy the underdeposit of ammonium chloride in the overhead equipment and piping in the refinery industry. This prospect of using GCI is based on the understanding that the extract exhibits necessary functional groups, including oxygen, sulfur, nitrogen, and their conjugation system [5]. The affinity of the highly electronegative atoms towards the metal restricts the proximity of oxygen gas to chlorides to form pitting corrosion [6] while replacing water molecules on the surface of metals to create a barrier layer [7].

Several authors have introduced the feasibility of demonstrating the GCI to limit pitting corrosion under ammonium chloride. A preliminary search was conducted by Ref. [8] to utilize the sodium dodecyl benzene sulfonate as a green corrosion inhibitor to mitigate zinc corrosion under 26 % NH_4Cl solution. It concludes that the inhibitor influences the anodic reaction with nearly 90 % inhibition efficiency at 298 K. The low inhibition efficiency of this study was improved by selecting chondroitin sulfate as an inhibitor. The authors in Ref. [9] elaborate on the formation of the dative covalent bond between the oxygen, sulfur, and nitrogen atoms to the vacant 3d-orbitals of Zinc, and the back-donate electrons via retro-donation become the prime factor in lowering the corrosion rate of zinc plate. Meanwhile, the paper of [10] examines the factors contributing to inhibition effectiveness in 7.5 % NH_4Cl. The research briefly discusses the imidazoline derivative effectively interfering with the anodic half-cell reaction with the predominant mixed-type inhibition process.

Based on the above publication, the selection of GCI is essential to remedy the corrosion threat under ammonium chloride. Importantly, none of the recent research extensively discussed the use of liquid smoke of rice husk ash (RHA) under 7.5 % NH_4Cl under an atmospheric condition, which may be suitable to remedy the corrosion in refinery types of equipment. This work aims to showcase the selection process of GCI using RHA to bridge the gaps in the previous research by providing comprehensive tests and characterization to unleash the potential of RHA as GCI. The objective and contribution of the study are as follows: Identifies the prime functional groups that influence corrosion inhibition through Fourier-transform infra-red (FTIR) and ultraviolet–visible (UV–Vis) spectroscopy. Discussing and analyzing the corrosion test result of potentiodynamic polarization (PDP) and electrochemical impedance spectroscopy (EIS). Elaborating and comparing the surface modification before and after the inhibitor is added as a qualitative and quantitative assessment.

However, the limitation of this paper is the corrosion simulation was conducted under atmospheric conditions, which may have variations when simulated in a CO_2-rich environment. It is noteworthy to claim that only the corrosion test curves displayed in this manuscript are measured at 323 K to showcase the inhibitor's thermal stability. In this instance, the RHA inhibitor comprises some active components/ingredients having divergent functional groups. Thus, probable temperature-induced decomposition of the RHA in the corrosive solution might generate individual inhibited species with higher activity at elevated temperatures, as they could adsorb on the metal surface facilely (with higher adsorption rate and less steric hindrance at the interface), leading to the formation of more compacted/denser inhibited film over it. Therefore, corrosion inhibition can be improved at elevated temperatures notwithstanding GCI's thermal stability.

It also restricts the discussion related to the effect of temperature on adsorption processes to unveil the types of adsorption. On top of that, the study has not specifically determined a possible molecular structure of RHA despite the previous research nuclear magnetic resonance (NMR) results indicating that the phenolic (3,5 dimethyl-phenol), carbonyl groups (2-Cyclopenten-1-one), siloxane (Tetracosamethyl-cyclododecasiloxane), and furan (2-ethyl-furan) are among the dominant molecules in RHA, as published in Ref. [11].

This study is organized to follow the flow of several sections. Section 1 introduces the motivation, novelty, and objective of the work. Section 2 provides the research methodology, while Section 3 shows a complementary result and discussion to simulate and evaluate the inhibitor's performance under the ammonium chloride test solution. Section 4 concludes the research.

2. Materials and methods

2.1. Prepared inhibitor and test solution

In this work, the inhibitor solution was prepared similarly to our previous work and published in Ref. [12] by condensing the vapor of rice husk waste through the pyrometallurgy process. Around fifty grams of the waste has undergone a reduction of their particle size

before being decomposed beyond 900 °C. The pyrolyzed RHA substance was transformed to provide pyrolytic gas, char, and smoke before cooling to 300 °C. The collected solution was allowed to cool to 25 °C. The blank test solution was prepared by adding analytical-grade ammonium chloride salt purchased from Merck. Co with purity of 99.8 % dissolved in distilled water (pH = 7.2). Three different inhibitor solutions were prepared by adding 2.5, 5, and 7.5 ppm of RHA in the uninhibited solution. The steel specimen was extracted from 5 mm of C1018 sample with percentage weight composition: C (0.198 wt%), Si (0.710 wt%), Mn (0.9046 wt%), Cr (0.151 wt%), and Fe (Bal.). The surface preparation was conducted by abrading the surface of the working electrode using SiC paper with grit number #400-#2000, cleaning it using ethanol, and storing it in desiccant to prevent atmospheric corrosion before utilizing it for the corrosion tests.

2.2. Corrosion tests

The primary intention of conducting a corrosion test is to assess the inhibitory performance of RHA under ammonium chloride solution at various concentrations. The composition of the cell comprises working, counter, and reference electrodes. The 0.5 cm thick square disk C1018 coupon was prepared, exhibiting a total area of 1 cm^2 embedded in epoxy resin and serving as a working electrode. The platinum wire has a 1 × 1 cm^2 area and was used as a counter electrode, and the reference electrode is saturated Ag/AgCl. The corrosion test, including potentiodynamic and electrochemical tests, was conducted using Gamry G-750, Gamry Instrument, Warminster, PA, USA series. The measurement used a potential of −250 mV to +250 mV at 1 mV/s to produce the Tafel curves. Equation (1) shows the corrosion inhibition efficiency calculation [13],

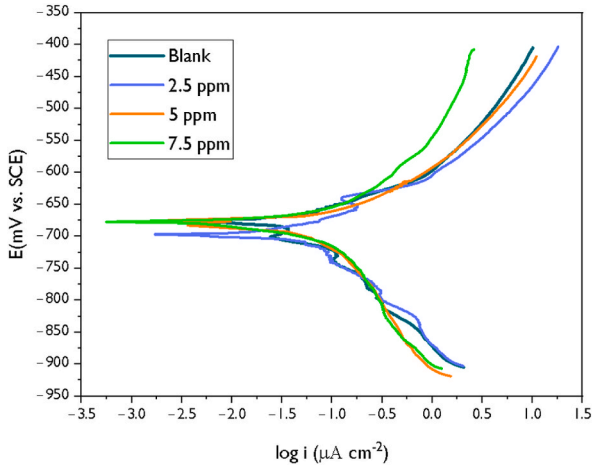

Fig. 1. Tafel polarization curves of RHA inhibitor at (a) various concentrations measured at 323 K and (b) various temperatures at 7.5 ppm RHA inhibitor.

$$\eta\% = \frac{(i_{untreated} - i)}{i_{untreated}} \times 100\% \quad (1)$$

In the above equation, η is the inhibition efficiency, $i_{untreated}$ and i are the corrosion current density before and after the inhibitor was added to the test solution. The electrochemical measurement was stabilized at an open circuit for 15 min. EC-Lab (version V10.40) was used to analyze the Tafel plots from the potential range. On the other hand, the electrochemical impedance spectrometer was utilized to evaluate the corrosion inhibition to produce Nyquist and Bode Plots and Bode Phase at 100 kHz to 0.2 Hz using the alternate current signal at 10 mV with 10 points/decade data recording. ZView freeware version 3.4e was carried out to analyze the EIS plots. Tafel and EIS measurements were conducted at 303, 313, and 323 K. However, the Tafel, Nyquist, and Bode Plots were reported in this work only at 323 K to unveil the inhibitor thermal stability under the NH_4Cl environment.

2.3. Surface morphology studies

In this work, the cleaned and dried electrodes were immersed in blank and 7.5 % NH_4Cl solution with 7.5 ppm RHA inhibitor added for 24 h at 303 K. In this case, the optimum immersion time is 24 h to allow the inhibitor to gradually detach from the metallic surface, which helps evaluate its film persistency [14]. After completion, the substrates were removed from the solutions, cleaned with distilled water and alcohol, and placed in the desiccator to free them from oxygen corrosion. The dominant compounds influencing the adsorption of the RHA substrate and their electronic transition related to inhibition were carried out using Fourier Transform-Infrared Spectroscopy (Thermo Scientific Nicolet iS-10) and Ultraviolet–visible (Shimadzu/UV-1201, Shimadzu Corp., Kyoto, Japan). On the other hand, the surface modification studies due to the film formation before and after the addition of RHA and their corresponding element types were studied using Scanning Electron Microscope-Energy Dispersive X-ray (SEM-EDX) of JEOL Type JSM 6390 and Atomic force microscopy (AFM) NX10 System, Park Systems Corp. Suwon, South Korea.

3. Results and discussion

3.1. Corrosion test result

Fig. 1 shows the result of potentiodynamic polarization measurement on various test solutions before and after the addition of inhibitors, which were measured at 323 K. In addition, Table 1 provides the kinetic parameters of the corrosion current density (i_{corr}), corrosion potential (E_{corr}), anodic and cathodic slope (β_a and β_c), corrosion rate, and inhibition efficiency calculated. The addition of RHA influences the cathodic and anodic regions with dominant in anodic.

Based on Fig. 1a, the C1018 material exhibited low corrosion current density in the presence of 7.5 ppm of RHA inhibitor to indicate the performance of inhibitor to retard the corrosion process and forms a barrier of passive film on the surface of the working electrode. On the other hand, the value of E_{corr} shifts to the positive regions, the corrosion current density decreases, and the difference between the highest and lowest potential value is lower than −85 mV to showcase the mixed-type inhibitor [15]. Accordingly, the movement of E_{corr} in a positive direction confirms the inhibitor works well as an anodic inhibitor [16].

Fig. 1b shows the Tafel polarization of 7.5 ppm RHA at various temperatures of 303–323 K to unveil the thermal characteristics and film stability of RHA. It is obvious, the trend for E_{corr} increases (−743.7 mV to −671.9 mV) as the temperature rises from 303 to 323 K and confirms the higher temperature leads to the susceptibility of working electrode to corrosion despite injection of inhibitor (see Fig. 1b) and confirms the higher corrosion rate from 0.013 mmpy to 0.120 mmpy (see Table 1) [17]. In consonance, the temperature remarkably influences the corrosion rate of C1018 based on the above investigation and lowers film stability. The facts align with the finding in Fig. 1a, to show a mixed-type inhibitor for RHA to reach maximum inhibition at 323 K although it has smaller inhibition efficiency at 313 K.

In the presence of an RHA inhibitor, the value of i_{corr} is inversely proportional to the value of R_{ct} and inhibition efficiency to confirm the inhibitive action of the RHA at the observable temperature. Moreover, the increased value of i_{corr} (0.849–7.027 μA/cm^2) by increasing in temperature corresponds to the lower thermal stability of inhibitors at higher temperatures and the loss of inhibitor

Table 1
The Potentiodynamic measurement result of RHA on the surface of C1018.

Conc (ppm)	Temp (K)	β_a (mV/decade)	β_c (mV/decade)	E_{corr} (mV vs. SCE)	i_{corr} (μA/cm^2)	*Chi-Square*	*Corr rate* (mmpy)	η (%)
Blank	303.0	55.7	82.3	−687.1	8.30	1.17	0.014	–
Blank	313.0	72.0	102.5	−697.4	18.64	1.56	0.031	–
Blank	323.0	98.2	126.6	−672.3	28.60	7.46	0.047	–
2.5	303.0	105.7	147.6	−692.9	3.080	2.79	0.051	62.89
2.5	313.0	85.2	195.2	−678.8	5.454	3.04	0.087	70.73
2.5	323.0	96.5	250.0	−682.4	7.360	3.94	0.167	74.27
5	303.0	70.2	25.8	−775.7	1.00	4.49	0.162	88.01
5	313.0	84.0	55.3	−743.7	8.40	2.13	0.130	54.93
5	323.0	71.6	93.7	−704.5	24.276	1.59	0.140	15.12
7.5	303.0	84.0	55.3	−743.7	0.849	2.13	0.013	89.77
7.5	313.0	114.0	153.0	−693.7	4.309	7.48	0.070	76.88
7.5	323.0	88.9	219.0	−671.9	7.027	2.45	0.120	96.41

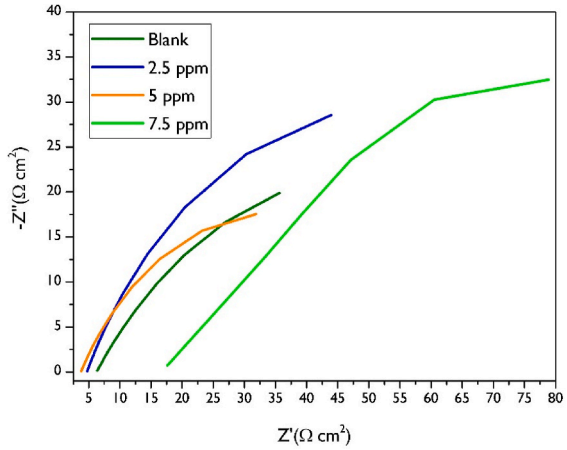

(a)

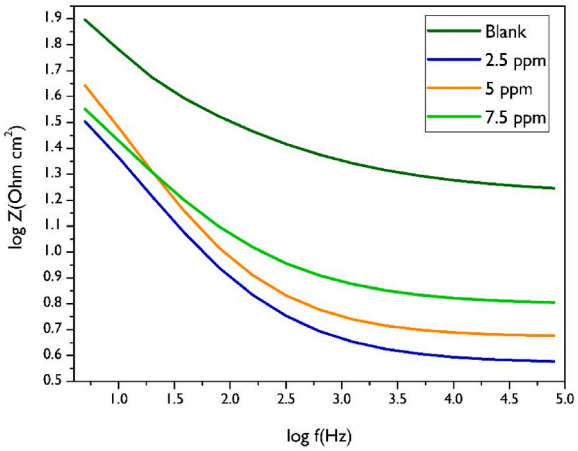

(b)

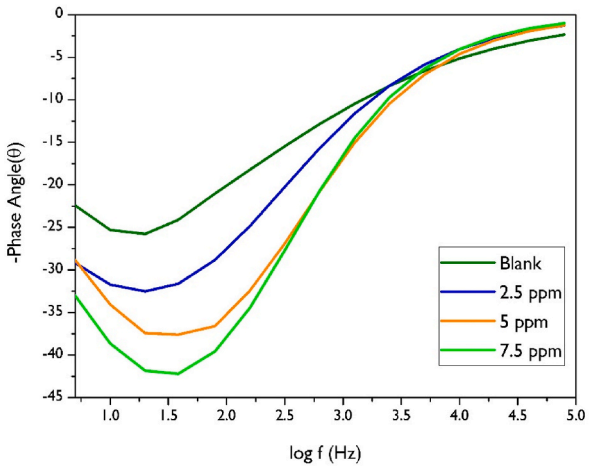

(c)

Fig. 2. The electrochemical test result of RHA on the surface of C1018 (a) Nyquist Plot (b) Bode Plot (c) Bode Phase measured at 323 K.

efficacy (see Fig. 1b) [18] despite the inhibitor remaining capable to quarantine the metal from the corrodent under NH_4Cl environment.

However, the decrease in the anodic slope (β_a) is more apparent than in the cathodic tafel slope (β_c) to, showcasing the inhibitor is anodically dominant. It also unveils that RHA alters the evolution of hydrogen and affects the dissolution of steel. Considering the variation value of β_a and β_c further confirms the physical and chemical adsorption of RHA to prohibit the electrochemical activity of C1018 steel from corrosion [19]. In addition, the corrosion current density (i_{corr}) shows a remarkable decrease as more concentrated inhibitor was added while raising the inhibition efficiency. In the blank solution, the i_{corr} value is 28.60 μA cm^{-2}, while the figure drops significantly to 1.027 μA cm^{-2} at 7.5 ppm RHA inhibitor. It shows that the RHA is suitable to depress the corrosion process despite a meaningful rise in corrosion rate.

According to the study [20], this value indicates a mixed-type inhibitor with a more significant effect in the anodic reaction. The optimum inhibition was achieved by adding a 7.5 ppm concentration of inhibitors. Table 1 confirms the result of Fig. 1 to unveil the irregular change value of Tafel slopes. The shape of curves is almost similar at the blank and various concentrations of the inhibited system. It implies that RHA does not change the chemical reaction in the interface between the metal and substrate and may similarly influence the cathodic and anodic [21]. With this in mind, the presence of RHA inhibits the dissolution of C1018 steel on the anodic site while reducing the hydrogen gas production in the cathode. The calculation of inhibition efficiency (by using equation (1)) at 7.5 ppm RHA at 323 K shows a higher value of 96.41 % compared to a non-inhibited system and provides a better inhibition on the surface of the substrate. When the concentration of RHA increases from 2.5 ppm to 5 ppm, a decline in inhibition efficiency is inevitable. It presumes that the steric effect hinders the formation of chemical bonding between the metal and RHA [22]. However, the higher concentration of 7.5 ppm shows the stability of the inhibitor increased and remained stable at 323 K. A lower chi-square test value also reveals the measurement's accuracy, low error, and high repeatability.

3.2. Electrochemical test

In this work, the Nyquist and Bode Plots and Bode Phase present the data on the performance of ammonium chloride with and without inhibitors. The EIS test is primarily beneficial for studying the properties before and after adsorption on the steel surface, covering the kinetic adsorption process. Fig. 2a shows the Nyquist plot of the untreated and treated solution using RHA as an inhibitor.

It is generally accepted that the EIS measurement is critical to acquire the adsorption dynamic process information when comparing the inhibitor performance added into the medium without and with the inhibitor. Fig. 2a shows the Nyquist plot when ammonium chloride is mixed at various concentrations. It was noticeable that the three inhibited systems had larger arc radii when the RHA inhibitor was added compared to the uninhibited system to show the passivation state and increase the resistivity of carbon steel [23].

It is also possible to note the loop at the high frequency corresponds to the Helmholtz plane and shows the presence of double-layer (C_{dl}) capacitance and increasing charge resistance (R_{ct}). While all the impedance spectra of electrochemicals show irregular semi-circles, the radius of the blank solution is shorter than the inhibited system as concentration remarkably increases. It confirms the value of R_{ct} increases as more reacting particles inhibit the charge transfer process on the metal's surface and indicates the occurrence of the inhibition process. Moreover, the Bode plot shows the increase of impedance of ($|Z|$) modulus value as concentration of RHA increases from 2.5 to 7.5 ppm (see Fig. 2b). The fact aligns with the increase of phase angle with higher dose of RHA concentration to increase the surface coverage of protection and to prove that the RHA inhibits the corrosion of AISI C1018. In this instance, the curve at 7.5 ppm widens compared to blank solution in the presence of RHA to suggest the one-time constant (see Fig. 2c) [24].With this in mind, the adsorption of RHA on the surface of AISI C1018 was further studied and confirmed.

It is possible to note the equivalent circuit model confirms the result shown in Table 2. In this instance, the circuit of the inhibited solution comprises R_s (solution resistance), R_{ct} (charge transfer resistance), and *CPE* (Constant Phase Element). In this model, the R_{ct} is in series with R_s while at the parallel with the *CPE*. The passive layer formation at RHS inhibitor is attributed to the value of R_{ct} (see Fig. 3) [25].

In this case, the one-time circuit diagram is more likely present as the formation passive layer may provide overlap in EIS response, as shown in Fig. 2 a-c [26–28]. Equation (2) shows the calculation of *CPE* (Z_{CPE}) [29].

Table 2
The EIS fitted electrochemical of RHA in NH_4Cl solution at various concentrations and temperature.

Conc (ppm)	Temp (K)	R_s (Ohm)	R_{ct} (Ohm)	n	Y_0 (Ω^{-1} s^n cm^{-1})	*Chi-square* (χ)	η (%)
Blank	303.0	22.57 ± 1.522	8.87 ± 0.453	0.4231 ± 0.0855	0.07997 ± 0.0570	0.0487	0.00
Blank	313.0	16.7 ± 1.030	6.139 ± 0.229	0.4031 ± 0.0650	0.10023 ± 0.0801	0.0252	0.00
Blank	323.0	16.40 ± 0.601	3.83 ± 0.2614	0.4171 ± 0.0236	0.08644 ± 0.0335	0.0173	0.00
2.5	303.0	4.53 ± 0.059	187.9 ± 0.161	0.6967 ± 0.0094	0.00091 ± 0.0053	0.0037	95.28
2.5	313.0	5.055 ± 0.102	115.9 ± 0.143	0.6831 ± 0.0179	0.00122 ± 0.0003	0.0106	94.70
2.5	323.0	6.2690 ± 0.183	89.27 ± 0.215	0.6863 ± 0.0156	0.00129 ± 0.0001	0.0080	95.71
5	303.0	11.5900 ± 0.606	77.16 ± 0.349	0.6326 ± 0.0851	0.00199 ± 0.0009	0.1280	88.50
5	313.0	3.8840 ± 0.101	57.7 ± 0.697	0.6678 ± 0.02412	0.00171 ± 0.0002	0.0163	89.36
5	323.0	3.7330 ± 0.092	62.73 ± 0.804	0.6534 ± 0.02234	0.00196 ± 0.00027	0.0137	93.90
7.5	303.0	2.57 ± 0.0467	78.18 ± 0.663	0.6201 ± 0.01154	0.00203 ± 0.00016	0.0041	88.65
7.5	313.0	6.621 ± 0.206	93.74 ± 0.235	0.5841 ± 0.03283	0.00250 ± 0.0005	0.0208	93.45
7.5	323.0	4.702 ± 0.081	98.55 ± 0.981	0.5830 ± 0.03071	0.00267 ± 0.0005	0.0181	96.12

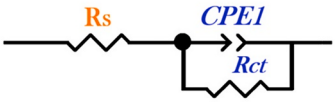

Fig. 3. The electrical equivalent diagram for the RHA inhibition of 7.5 ppm measured at 323 K.

$$Z_{CPE} = \frac{1}{(Y_0)(j\omega)^n} \tag{2}$$

In the above equation (Equation (2)), Y_0 is the passivity of the system, j is the imaginary number, and n is the phase shift related to surface heterogeneity. Table 2 shows the fitted value of impedance, including Constant Phase Element (Y_o and n). In this case, the system passivity corresponds to the value of *CPE*.

The rise of the n value corresponds to the increase of surface inhomogeneity and is a provision to describe the film formation of inhibitor on the surface of the working electrode (see Table 2) and attributed to the *CPE* circuit as illustrated in Fig. 3b [30]. The decrement of Y_0 values can be attributed to more displacement of water molecules with RHA inhibitors in the double layer formed at the interface, shown by the change in their value from 0.08644 ± 0.0335 Ω^{-1} sn cm^{-1} to 0.00267 ± 0.0005 Ω^{-1} sn cm^{-1}.

Equation (3) shows the calculation of inhibition efficiency based on the impedance measurement [31],

$$\%\eta = \frac{R_{ct} - R_s}{R_{ct}} \times 100\% \tag{3}$$

In the above equation (Equation (3)), R_{ct} and R_s are the charge transfer and solution resistant to unveil the inhibited and uninhibited resistance.

This trend aligns with the decline of R_s and the increasing value of R_{ct} to confirm that inhibition occurs on the metal surface and replaces more water molecules. Without inhibitor at 323 K, the value of R_{ct} is 3.83 ± 0.2614 Ω and increases steadily to 98.55 ± 0.981 Ω to show the formation of the passive layer to protect the metal from further dissolution and confirms the rise of inhibition efficiency to 96.12 % at 7.5 ppm RHA measured at 323 K. In this instance, despite raising the temperature to 323 K, the inhibitor effectively lowers the corrosion rate and provides a better adsorption quality, as shown by the higher inhibition efficiency.

Nonetheless, the result can be used as a model to scale up the green corrosion inhibitor to achieve identical inhibition efficiency when it simulates under turbulent multiphase flow where the amine derivates compound such as the utilization of imidazoline as corrosion inhibitor in the industrial setting. According to the report in Ref. [32], the higher dose of imidazoline 500 ppm was used to achieve maximum inhibition at 97 %. Moreover, at higher temperatures and concentrations, the prospect of inhibitors is evident and comparable to the work of [33]. They report the green inhibitor based on ammonia, organic amines, amides, and imidazolines was evaluated to protect the overhead equipment and shows the corrosion rate at < 0.13 mmpy.

With this in mind, the potential utilization of RHA in the overhead refinery unit is feasible as they present an identical corrosion rate at 0.125 mmpy when adding a 7.5 ppm inhibitor at 323 K. High thermal stability becomes a primary factor in selecting inhibitors in this refinery unit. Moreover, the low chi-square (χ) relates to the fitted calculation, agrees with the experimental result, and exhibits high-quality fitting.

In the presence of an RHA inhibitor, the capacitance arc reactant's radius increases remarkably than that of the blank and inhibitor concentrations. In consonance, this behavior corresponds to the more prominent inhibition while increasing the charge transfer resistance, as depicted in Table 2. At the highest inhibitor concentration, the flat semicircles appear due to the dispersion effect as more

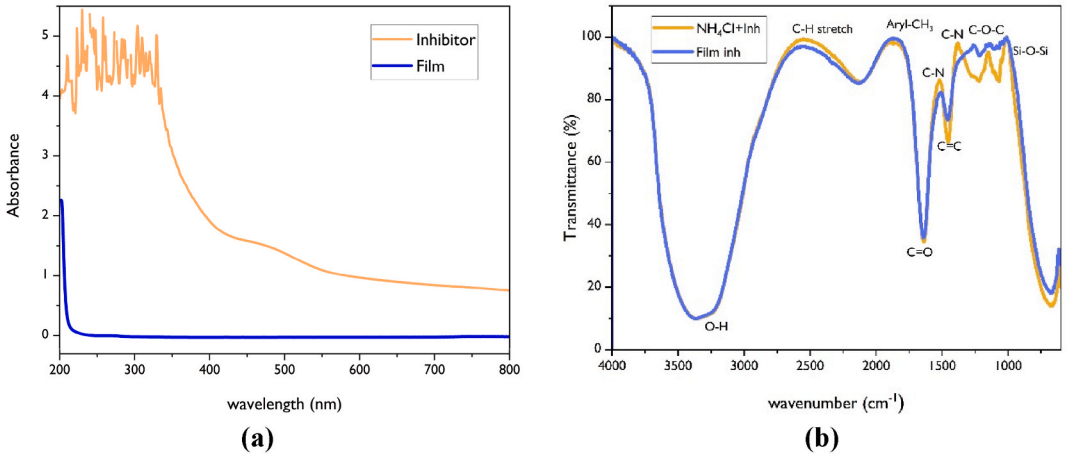

Fig. 4. The result of (a) UV–Vis Spectrum (b) functional groups evaluation of 7.5 ppm RHA.

heterogenous substances are adsorbed while smoothening the surface of working electrodes [19].

3.3. FTIR and UV–vis test results

Fig. 4 shows the composition of the blank and inhibited solution that the FTIR and UV–Vis analyzed. The tests are essential to unveil the adsorption of organic molecules from RHA inhibitors on the surface of C1018 steel. Furthermore, the test is available to verify the type of functional groups in the form of the aromatic ring, heteroatoms, and double bonds, which correspond to the formation of inhibited film as modeled in Fig. 3b. The absorption spectra of the RHA in the inhibitor solution and on the inhibited film were recorded in Fig. 4a. By observing the figure, the UV–Vis spectrum of RHA shows an intensive peak absorption. It is possible to note that the peak at approximately 220–230 nm disappeared from the inhibitor to the surface of the inhibited film. In this instance, the intense absorption peak appears to be correlated to the electronic transition from π–π* from the inhibitor due to the adsorption of the C═C conjugate bond in the aromatic ring [34].

Accordingly, a weaker intensive absorption peak at approximately 270–280 nm occurs due to the transition of n–π* from the C═O. Also, the disappearance of the peak around 320 nm is attributed to the film formation associated with the electronic transition from the conjugated C═C and C═O, primarily adsorbed from the RHA inhibitor on the working electrode [28]. It is predicted to react with the dissolved iron and form the Fe-Inh complex.

The result of UV–Vis aligns with the functional group test result, as illustrated in Fig. 4b. It is possible to note that the major groups of RHA in the test solution (NH_4Cl with inhibitor) show the absorption of several functional groups. The appearance absorption peaks of –OH, C–H stretch, Aryl-CH_3, C═O, C═C, C–N, C–*O*–C, and Si–*O*–Si were significant and shifted the location compared to the pure NH_4Cl + inhibitor spectra as illustrated in Fig. 4b. For instance, the peak appearance at 3500 cm^{-1} correlates to the stretching bond of –OH [35] in the extracted film and the test solution. The peak corresponds to the inhibition activity of 3,5 dimethyl-phenol, which actively donates its lone pair of electrons to positive ions of metal [36]. The C–H stretch peak appears and shifts to 2866 cm^{-1} from 2870 cm^{-1}, while no such shifting for the Aryl-CH_3 and C═O. The two functional groups completely disappeared from inhibitor to inhibited film at 2950-2850 and 1500-1600 cm-1, which can be attributed to the adsorption of 2-cyclopenten-1-one molecules [37]. The disappearance may also related to their strong reaction to the C1018 steel.

Another shifting appearance is evident in C–N, aromatic C═C, and C–*O*–C, shown by the peak approximately at 1540 cm^{-1}, 1510 cm^{-1}, and 1120 $cm^{-1,}$ similar to the results in Refs. [38,39]. The functional groups of C–N can be associated with the participation of 2-methyl-pyridine in the inhibition process. While the height of the C═C absorption peak is confirmed and decreased at around 1493 cm^{-1} and confirms the peak of UV–Vis at 280–320 nm, it provides the possibility of electron donation from inhibitor to steel and indicates the adsorption of inhibitor molecules on the surface of the metal. It is possible since the transition of π–π* conjugation shows the chelation process between the Fe and RHA inhibitor to confirm the UV–vis result (see Fig. 4a). In addition, no transition shift peak of Si–*O*–Si at 1100 cm^{-1} to elucidate the unreactive properties of tetracosamethyl-cyclododecasiloxane and forms non-hydrophilic properties on the metallic surface and to replace more water molecules and increases the hydrophobicity of the substrate [40].

The obtained functional groups in this study align with the result of [41], which argues that nitrogenated-containing compounds such as 2-ethyl-furan of RHA are suitable for practical application to protect petrochemical refineries. Accordingly, the study [42] shows that amines-derivate compounds are commonly used in industry to reduce overhead corrosion under low temperatures and conform to the result of EIS when 7.5 ppm of RHA inhibitor is added at 303 K as a comparison to the requirement of corrosion inhibitor in practical (see Table 2). Likewise, the presence of 3,5 dimethyl-phenol can be associated with the potent performance of RHA to be efficient in refineries at small doses to mitigate the corrosion in the process stream refineries.

3.4. Surface modification result

Fig. 5 showed the result of surface studies when the C1018 steel was at different conditions (immersed in the NH_4Cl solution and the

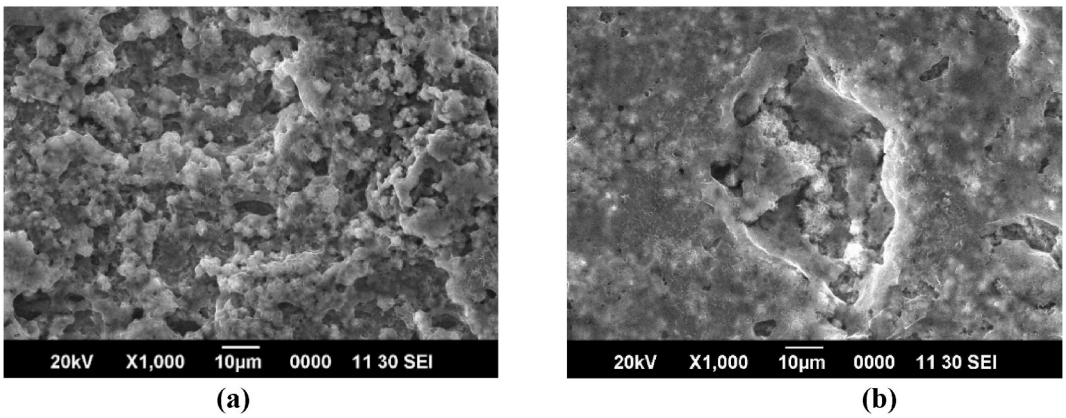

Fig. 5. The surface morphology-elemental analysis result (a) uninhibited, (b) inhibited system.

test solution comprised NH_4Cl and RHA inhibitor). Also, the AFM micrographs are provided further to study the corrosion process in mild steel.

Without inhibitors, the surface of the steel is remarkably damaged and damaged in the spherical form, growing out in voids and forming a bundling compact structure (Fig. 5a). It is evident that the corroded surface is considered as damaged of the smooth surface C1018 as can be seen from the coupon exposed in NH_4Cl solution. On the other hand, a cleaner and smoother surface of the mild steel was observed after being immersed in the RHA inhibitor. It is possible to observe the fine holes and fewer cracks prominently appearing on the steel (Fig. 5b). Hence, it is clear that the addition of inhibitor modifies the corroded steel surface, and the results are aligned with the corrosion.

Identifying elemental composition is essential to locate the source of damage on the coupon through EDX analysis (see Table 3). In the uninhibited system, the chloride ions penetrate the metal surface and form an oxidation layer to confirm the corrosion process. As depicted in Fig. 5a, the worn C1018 metal is covered by a fragile oxide layer as a high content of oxygen is observed (8.63 % weight and 23.85 % atoms).

Likewise, adding 7.5 ppm of inhibitor solution lowers the amount of chloride and oxygen to prove the inhibition reaction was slower. The inhibitor serves as a barrier to prevent direct contact between the metal and the environment (NH_4Cl solution) by forming a protective layer on the steel surface [43]. This phenomenon is supported by the low Fe/O ratio of inhibited systems. In the blank solution, the Fe/O ratio was 9.82 and declined to 7.22 when the inhibitor was injected into the test solution. In general, the depression creation of iron oxides/hydroxide as a corrosion product elicits the adsorption of inhibitor.

In this work, the Atomic Force Microscope (AFM) micrographs and their respective skewness and roughness values for the steel immersed in NH_4Cl before and after the addition of inhibitor are reported in Fig. 6. The micrograph shows the value of maximum height peak roughness R_p and root mean square roughness R_q remarkably decreases by nearly 30 % after addition of inhibitor. It reflects the formation of a protective layer on the mild steel, reduces the oxidation of iron to dissolve into the solution, and decreases the damage on the surface [44]. The quantitative result agrees well with the surface's smoother surface as the depth of the layer of the immersed coupon in inhibitor solution is lower than that of in the absence of inhibitor.

The uninhibited system's irregular morphology shows a deeper valley due to corrosion. The possible corrosion products absorbed on the coupon correspond to the FeOH, FeOOH, and $FeCl_3$, as depicted in the EDX result (see Fig. 5) [43]. With inhibitors, the coupon C1018 substrate receives considerable protection as a smoother surface substrate appears where the number of peaks is dominant compared to the valley. In this case, forming the Fe-(NH_4Cl-RHA)n complex is possible as more inhibitor molecules progressively block the active sites and depress the corrosion.

3.5. Proposed inhibition mechanism

The inhibition mechanism of RHA might be explained as the adsorption of the liquid smoke of RHA on the anodic regions of C1018 to establish an inhibited film that limits the electrochemical activity and increases the strength of protection from ammonium chloride. Therefore, the possible inhibition at the cathode and anode of the RHA is the following:

$$Cathode: 2H^{+}_{(aq)} + 2e^{-} \leftrightarrow H_{2(aq)}$$
$$RHA_{(aq)} + H^{+}_{(aq)} \leftrightarrow RHAH^{+}_{(aq)}$$
$$RHAH^{+}_{(aq)} \leftrightarrow RHAH^{+}_{(s)}$$
$$Anode: Fe_{(s)} \rightarrow Fe^{2+}_{(aq)} + 2e^{-}$$
$$RHA_{(aq)} + nFe^{2+}_{(aq)} + NH_4Cl_{(aq)} \leftrightarrow \left[(Fe - NH_4Cl - RHA)_n\right]_{(aq)}$$
$$\left[(Fe - NH_4Cl - RHA)_n\right]_{(aq)} \leftrightarrow \left[(Fe - NH_4Cl - RHA)_n\right]_{(s)}$$

At the cathode, the RHA inhibits the evolution of hydrogen ion into hydrogen gas and it assumes that the solidification of inhibitor occurs. On the other hand, the formation of complex compound of [(Fe–NH_4Cl-RHA)$_n$] confirms the surface modification of the working electrode as illustrated in Figs. 5b and 6b.

A possible process begins from the interaction between positive metal ions with the anions from RHA [45], and the predicted participating molecules are 2-ethyl furan and tetracosamethyl-cyclododecasiloxane (see Fig. 7).

In short, the physiosorption is governed by the van der Waals forces between long chains of Si–*O*–Si to allow the inhibitor coated on the metal surface due to adsorption to displace more water molecules and increase potential protection [46].

In addition, the presence of phi (π) bond in 3,5 dimethyl-phenol and 2-cyclopenten-1-one, is suggested to be involved in the inhibition process when the sideways p-orbital of inhibitors molecule on the oxygen atom in 2-cyclopenten-1-one and π-electrons in the

Table 3
The elemental composition of the C1018 surface before and after inhibition.

Element	Uninhibited System		Inhibited System	
	Mass (%)	Atoms (%)	Mass (%)	Atoms (%)
O	8.63	23.85	10.23	27.06
Cl	8.44	10.52	10.89	13.00
Fe	82.92	65.63	78.63	59.57

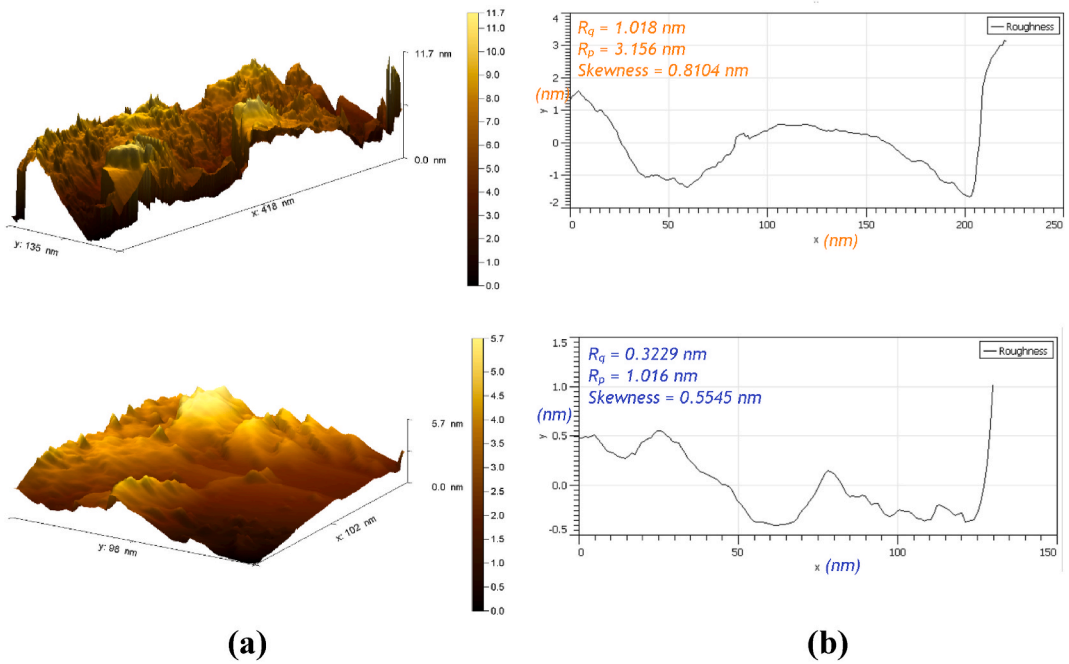

Fig. 6. The surface morphology result (a) uninhibited, (b) inhibited system.

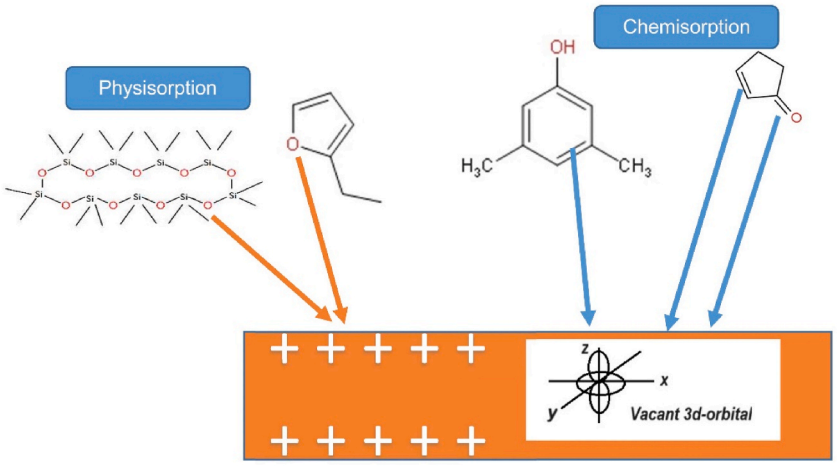

Fig. 7. The proposed inhibition mechanism of RHA.

resonance system of 3,5 dimethyl-phenol increases electron donation possibility to form chemical bonding through the formation of complex compound. It is noteworthy to remember that the resonance system in the benzene ring of the above molecules increases the partial positive charge over the molecule. In this circumstance, the inhibitor readily accepts released electrons when the metal is exposed to corrodent [47]. It forms a complex compound between metal and inhibitor by forming a dative covalent bond. The predicted inhibition mechanism shown in Fig. 7 aligns with the result in Table 2 of low corrosion rate. In addition, it is assumed that the inhibitor is parallelly oriented on the surface of C1018 and prevents them from corrosion.

4. Conclusion

The research has primarily paved the way for studying corrosion prevention in mild steel C1018 as a green corrosion inhibitor. The existing study shows that the effectiveness of RHA is essential to developing the life-limiting failure mechanism of corroded materials. The result of the potentiodynamic shows the depression of the corrosion current density to 28.60 μA cm^{-2} becomes the foundation knowledge that the inhibitor contributes to decreasing the degradation rate of the material. As the current corrosion density decreases,

the inhibition efficiency increases by greater than 96 % for potentiodynamic and electrochemical tests. The inhibitor influences the reaction at the anode and cathode with the dominant anodic type at 313 K and gradually decrease in their inhibitory effect at 323 K. Based on the Nyquist plot, the increase in the semi-arc Nyquist graph shows the extensive protection of the metal. The Bode Plot and Phase agree well with the Nyquist plot, which shows the maximum protection when a 7.5 ppm RHA inhibitor was added to the test solution. The transition of electrons from n–π^* and π –π^* confirms the presence of functional groups C═C, C═O, and –OH as the ultimate functional group to increase the electron donation from inhibitor to metallic site. As a result, the adsorption of the inhibited layer has modified the surface of the metal to provide a smoother surface with a lower value of chloride and oxygen in the inhibited system.

Financial Support

The authors gratefully thank to the University of Indonesia under the PUTI Pascasarjana grant year of 2023–2024 with contract number NKB-257/UN2.RST/HKP.05.00/2023. Our extensive appreciation is given to Fiona Hiu from National High School Jakarta for her overall contribution to collecting the corrosion test data.

Data availability statement

The data that has been used is confidential.

CRediT authorship contribution statement

Agus Paul Setiawan Kaban: Writing – original draft, Visualization, Methodology, Formal analysis, Data curation, Investigation, Resources, Writing – review & editing. **Johny Wahyuadi Soedarsono:** Writing – review & editing, Methodology, Investigation, Funding acquisition, Conceptualization. **Mochammad Syaiful Anwar:** Methodology, Investigation, Data curation, Conceptualization. **Wahyu Mayangsari:** Methodology, Investigation, Data curation. **Ahmad Maksum:** Resources, Investigation, Data curation. **Aga Ridhova:** Resources, Investigation, Formal analysis, Data curation. **Rini Riastuti:** Writing – review & editing, Methodology, Funding acquisition, Conceptualization. **Dedy Iskandar:** Resources, Methodology, Formal analysis, Data curation. **Ayende:** Writing – review & editing, Funding acquisition, Formal analysis, Conceptualization, Writing – review & editing, Funding acquisition, Formal analysis, Conceptualization.

Declaration of competing interest

The authors declare that they have no known competing financial interests or personal relationships that could have appeared to influence the work reported in this paper.

References

[1] A.H. Al-Moubaraki, I.B. Obot, Corrosion challenges in petroleum refinery operations: sources, mechanisms, mitigation, and future outlook, J. Saudi Chem. Soc. (2021), https://doi.org/10.1016/j.jscs.2021.101370.
[2] K. Toba, M. Ueyama, K. Kawano, J. Sakai, Corrosion of carbon steel and alloys in concentrated ammonium chloride solutions, Corrosion (2012), https://doi.org/10.5006/0587.
[3] A. Groysman, Corrosion problems and solutions in oil, gas, refining and petrochemical industry, Koroze a Ochr. Mater (2017), https://doi.org/10.1515/kom-2017-0013.
[4] M.A. Chidiebere, E.E. Oguzie, L. Liu, Y. Li, F. Wang, Ascorbic acid as corrosion inhibitor for Q235 mild steel in acidic environments, J. Ind. Eng. Chem. (2015), https://doi.org/10.1016/j.jiec.2014.11.029.
[5] K. Kanayo Alaneme, S. Joseph Olusegun, Corrosion inhibition performance of lignin extract of sun flower (tithonia diversifolia) on medium carbon low alloy steel immersed in H2SO4 solution, Leonardo J. Sci. 11 (20) (2012) 59–70.
[6] K. Habib, In-situ monitoring of pitting corrosion of copper alloys by holographic interferometry, Corros. Sci. (1998), https://doi.org/10.1016/S0010-938X(98)00049-3.
[7] M. Finšgar, J. Jackson, Application of corrosion inhibitors for steels in acidic media for the oil and gas industry: a review, Corrosion Sci. (2014), https://doi.org/10.1016/j.corsci.2014.04.044.
[8] Y. Qiang, et al., Sodium dodecyl benzene sulfonate as a sustainable inhibitor for zinc corrosion in 26% NH4Cl solution, J. Clean. Prod. (2017), https://doi.org/10.1016/j.jclepro.2017.03.104.
[9] A. Singh, K.R. Ansari, M.A. Quraishi, Chondroitin sulfate as a green corrosion inhibitor for zinc in 26% ammonium chloride solution: electrochemical and surface morphological analysis, Colloids Surfaces A Physicochem. Eng. Asp. (2020), https://doi.org/10.1016/j.colsurfa.2020.125465.
[10] A. Munis, T. Zhao, M. Zheng, A.U. Rehman, F. Wang, A newly synthesized green corrosion inhibitor imidazoline derivative for carbon steel in 7.5% NH4Cl solution, Sustain. Chem. Pharm. (2020), https://doi.org/10.1016/j.scp.2020.100258.
[11] R. Kaban, A, W. Mayangsari, M. Anwar, A. Maksum, T. Aditiyawarman, J. Soedarsono, A. Ridhova, Riastuti, Unraveling the study of liquid smoke from Rice Husks as a green corrosion inhibitor in mild steel under 1 M HCl, Eastern-European J. Enterp. Technol. 5 (2022), https://doi.org/10.15587/1729-4061.2022.265086.
[12] M. S. A., A. Paul Setiawan Kaban, W. Mayangsari, et al., Experimental and modelling waste rice husk ash as a novel green corrosion inhibitor under acidic environment, Mater. Today Proc. (2022) 1–10, https://doi.org/10.1016/j.matpr.2022.04.738.
[13] J. Xu, R. Jia, D. Yang, C. Sun, T. Gu, Effects of D-Phenylalanine as a biocide enhancer of THPS against the microbiologically influenced corrosion of C1018 carbon steel, J. Mater. Sci. Technol. (2019), https://doi.org/10.1016/j.jmst.2018.09.011.
[14] Z. Zhou, X. Min, S. Wan, J. Liu, B. Liao, X. Guo, A novel green corrosion inhibitor extracted from waste feverfew root for carbon steel in H2SO4 solution, Results Eng (2023), https://doi.org/10.1016/j.rineng.2023.100971.
[15] R. Haldhar, et al., Investigation of plant waste as a renewable biomass source to develop efficient, economical and eco-friendly corrosion inhibitor, J. Mol. Liq. (2021), https://doi.org/10.1016/j.molliq.2021.116184.

[16] M.A. Deyab, B. El Bali, R. Essehli, R. Ouarsal, M. Lachkar, H. Fuess, NaNi(H2PO3)3·H2O as a novel corrosion inhibitor for X70-steel in saline produced water, J. Mol. Liq. (2016), https://doi.org/10.1016/j.molliq.2016.01.075.
[17] A.M. Abdel-Gaber, A. Ezzat, M.E. Mohamed, Fenugreek seed and cape gooseberry leaf extracts as green corrosion inhibitors for steel in the phosphoric acid industry, Sci. Rep. (2022), https://doi.org/10.1038/s41598-022-26757-z.
[18] F.M. Ibrahim, R.A. Hammza, D.H. Fadhil, Synthesis and characterization of Trimethoprim metal complexes used as corrosion inhibitors for carbon steel in acid media, Int. J. Corros. Scale Inhib. (2019), https://doi.org/10.17675/2305-6894-2019-8-3-20.
[19] A. Farhadian, et al., Modified hydroxyethyl cellulose as a highly efficient eco-friendly inhibitor for suppression of mild steel corrosion in a 15% HCl solution at elevated temperatures, J. Mol. Liq. (2021), https://doi.org/10.1016/j.molliq.2021.116607.
[20] Z. Pilić, I. Martinović, Effect of Helichrysum italicum on the corrosion of copper in simulated acid rain solution, Chem. Biochem. Eng. Q. (2020), https://doi.org/10.15255/CABEQ.2019.1614.
[21] C.S. Proença, B. Serrano, J. Correia, M.E.M. Araújo, Evaluation of tannins as potential green corrosion inhibitors of aluminium alloy used in aeronautical industry, Metals (2022), https://doi.org/10.3390/met12030508.
[22] L. Huang, H.J. Li, Y.C. Wu, Comprehensive evaluation of corrosion inhibition performance and ecotoxicological effect of cinchona IIa as a green corrosion inhibitor for pickling of Q235 steel, J. Environ. Manage. (2023), https://doi.org/10.1016/j.jenvman.2023.117531.
[23] M.A. Deyab, E. Guibal, Enhancement of corrosion resistance of the cooling systems in desalination plants by green inhibitor, Sci. Rep. (2020), https://doi.org/10.1038/s41598-020-61810-9.
[24] Y. Yu, D. Yang, D. Zhang, Y. Wang, L. Gao, Anti-corrosion film formed on HAl77-2 copper alloy surface by aliphatic polyamine in 3 wt.% NaCl solution, Appl. Surf. Sci. (2017), https://doi.org/10.1016/j.apsusc.2016.09.118.
[25] M. El Faydy, et al., An experimental-coupled empirical investigation on the corrosion inhibitory action of 7-alkyl-8-Hydroxyquinolines on C35E steel in HCl electrolyte, J. Mol. Liq. (2020), https://doi.org/10.1016/j.molliq.2020.113973.
[26] A.R. Kaban, Agus Paul Setiawan, Johny Wahyuadi Soedarsono, Wahyu Mayangsari, Mochamad Syaiful Anwar, Ahmad Maksum, Rini Riastuti, Insight on corrosion prevention of C1018 in 1.0 M hydrochloric acid using liquid smoke of rice husk ash: electrochemical, surface analysis, and deep learning studies, Coatings, MDPI 13 (1) (2023), https://doi.org/10.3390/coatings13010136.
[27] D. Marunkić, et al., Inhibitory effect of cerium salts of lower carboxylic acids on Al-Zn-Mg-Cu alloy in NaCl solution, J. Electrochem. Soc. (2021), https://doi.org/10.1149/1945-7111/ac1895.
[28] J.A. Hill, T. Markley, M. Forsyth, P.C. Howlett, B.R.W. Hinton, Corrosion inhibition of 7000 series aluminium alloys with cerium diphenyl phosphate, J. Alloys Compd. (2011), https://doi.org/10.1016/j.jallcom.2010.09.151.
[29] Y. Kerroum, A. Guenbour, A. Bellaouchou, H. Idrissi, J. Garcia-Anton, A. Zarrouk, Chemical and physical effects of fluoride on the corrosion of austenitic stainless steel in polluted phosphoric acid, J. Bio- Tribo-Corrosion (2019), https://doi.org/10.1007/s40735-019-0261-5.
[30] Q. Zhao, J. Guo, G. Cui, T. Han, Y. Wu, Chitosan derivatives as green corrosion inhibitors for P110 steel in a carbon dioxide environment, Colloids Surfaces B Biointerfaces (2020), https://doi.org/10.1016/j.colsurfb.2020.111150.
[31] Y. Lekbach, et al., Green corrosion inhibition and adsorption behaviour of cistus ladanifer extract on 304L stainless steel in hydrochloric acid solution, Arab. J. Sci. Eng. (2021), https://doi.org/10.1007/s13369-020-04791-1.
[32] Robin D Term, Ammonium Bisulfide Corrosion in Hydrocracker and Refinery Sour Water Service, Saudi Arabia, 2004.
[33] A. Groysman, L. Mizrahi, J. Penner, N. Brodsky, Examination of a 'green' Corrosion Inhibitor and Corrosion Resistant Alloys for the Overhead of the Crude Oil Distillation Unit, 2013.
[34] A. Sedik, et al., Dardagan Fruit extract as eco-friendly corrosion inhibitor for mild steel in 1 M HCl: electrochemical and surface morphological studies, J. Taiwan Inst. Chem. Eng. 107 (2020) 189–200, https://doi.org/10.1016/j.jtice.2019.12.006.
[35] A.P.S. Kaban, et al., Development of white tea extract as green corrosion inhibitor in mild steel under 1 M hydrochloric acid solution, Eastern-European J. Enterp. Technol. (2021), https://doi.org/10.15587/1729-4061.2021.224435.
[36] A. Samide, B. Tutunaru, A. Moanță, C. Ionescu, C. Tigae, A.C. Vladu, A study of the surface protective layer formed on carbon steel in water-dioxane solution containing 0.15 M NaCl in presence of an azo dye with antimicrobial activity, Int. J. Electrochem. Sci. (2015), https://doi.org/10.1016/s1452-3981(23)06652-x.
[37] H.U. Nwankwo, L.O. Olasunkanmi, E.E. Ebenso, Electrochemical and computational studies of some carbazole derivatives as inhibitors of mild steel corrosion in abiotic and biotic environments, J. Bio- Tribo-Corrosion (2018), https://doi.org/10.1007/s40735-018-0130-7.
[38] M. Mecozzi, M. Pietroletti, M. Scarpiniti, R. Acquistucci, M.E. Conti, Monitoring of marine mucilage formation in Italian seas investigated by infrared spectroscopy and independent component analysis, Environ. Monit. Assess. (2012), https://doi.org/10.1007/s10661-011-2400-4.
[39] A.O. Balogun, O.A. Lasode, H. Li, A.G. McDonald, Fourier transform infrared (FTIR) study and thermal decomposition kinetics of sorghum bicolour glume and albizia pedicellaris residues, Waste and Biomass Valorization (2015), https://doi.org/10.1007/s12649-014-9318-3.
[40] C.F. Lin, W.T. Tseng, M.S. Feng, Formation and characteristics of silicon nanocrystals in plasma-enhanced chemical-vapor-deposited silicon-rich oxide, J. Appl. Phys. (2000), https://doi.org/10.1063/1.372260.
[41] P. Topilnitskij, Corrosion protection of oil production and refinery equipment, Chem. Chem. Technol. (2007), https://doi.org/10.23939/chcht01.01.045.
[42] Corrosion in the Petrochemical Industry, 2020.
[43] X.Y. Shao, W.Y. Hanlin, Kegui Zhang, Y. Liu, N-[2-(3-indolyl)ethyl]-cinnamamide synthesized from cinnamomum cassia presl and alkaloid tryptamine as green corrosion inhibitor for Q235 steel in acidic medium, J. Mater. Res. Technol. 20 (2022) 916–933, https://doi.org/10.1016/j.jmrt.2022.07.122.
[44] N. Asadi, M. Ramezanzadeh, G. Bahlakeh, B. Ramezanzadeh, Utilizing Lemon Balm extract as an effective green corrosion inhibitor for mild steel in 1M HCl solution: a detailed experimental, molecular dynamics, Monte Carlo and quantum mechanics study, J. Taiwan Inst. Chem. Eng. (2019), https://doi.org/10.1016/j.jtice.2018.07.011.
[45] M. I. N., A.G. Raghda A. El-Nagar, N.A. Khalil, Y. Atef, Evaluation of ionic liquids based imidazolium salts as an environmentally friendly corrosion inhibitors for carbon steel in HCl solutions, Sci. Rep. 14 (2024), https://doi.org/10.1038/s41598-024-52174-5.
[46] A.S. Fouda, S.A.A. El-Maksoud, A.T. El-Habab, A.R. Ibrahim, Synthesis and characterization of novel fatty alcohol ethoxylate surfactants for corrosion inhibition of mild steel, J. Bio- Tribo-Corrosion (2021), https://doi.org/10.1007/s40735-020-00448-6.
[47] L. Zhang, et al., A novel imidazoline derivative as corrosion inhibitor for P110 carbon steel in hydrochloric acid environment, Petroleum (2015), https://doi.org/10.1016/j.petlm.2015.10.007.